

Zero Energy Peak and Triplet Correlations in Nanoscale *SFF* Spin-Valves

Mohammad Alidoust,^{1,*} Klaus Halterman,^{2,†} and Oriol T. Valls^{3,‡}

¹*Department of Physics, University of Basel, Klingelbergstrasse 82, CH-4056 Basel, Switzerland*

²*Michelson Lab, Physics Division, Naval Air Warfare Center, China Lake, California 93555, USA*

³*School of Physics and Astronomy, University of Minnesota, Minneapolis, Minnesota 55455, USA*

(Dated: March 5, 2022)

Using a self-consistent Bogoliubov-de Gennes approach, we theoretically study the proximity-induced density of states (DOS) in clean *SFF* spin-valves with noncollinear exchange fields. Our results clearly demonstrate a direct correlation between the presence of a zero energy peak (ZEP) in the DOS spectrum and the persistence of spin-1 triplet pair correlations. By systematically varying the geometrical and material parameters governing the spin-valve, we point out to experimentally optimal system configurations where the ZEPs are most pronounced, and which can be effectively probed via scanning tunneling microscopy. We complement these findings in the ballistic regime by employing the Usadel formalism in the full proximity limit to investigate their diffusive *SFF* counterparts. We determine the optimal normalized ferromagnetic layer thicknesses which result in the largest ZEPs. Our results can serve as guidelines in designing samples for future experiments.

PACS numbers: 74.50.+r, 74.25.Ha, 74.78.Na, 74.50.+r, 74.45.+c, 74.78.FK, 72.80.Vp, 68.65.Pq, 81.05.ue

I. INTRODUCTION

The interplay of ferromagnetism and superconductivity in hybrid superconductor (*S*) ferromagnet (*F*) structures (*S/F* structures) constitutes a controllable system in which to study fundamental physics, including prominently that of competing multiple broken symmetries.^{1,2} The proximity of a conventional *s*-wave superconductor with non-aligned ferromagnetic layers, or a textured ferromagnet, induces both spin-singlet and odd frequency³ (or equivalently odd-time⁴) spin-triplet correlations with 0 and ± 1 spin projections along a spin quantization axis. These triplet pairs stem from broken time reversal and translations^{1,2} symmetries. This kind of spin-triplet pairings originally suggested as a possible pairing mechanism in ³He,³ has reportedly been observed in intermetallic compounds such as Sr₂RuO₄.^{5,6} *SF* heterostructures are particularly simple and feasible experimental systems which allow for direct studies of the intrinsic behavior of differing superconducting pairings. Unlike the opposite-spin correlations, spin-1 pairing correlations are rather insensitive to the pair-breaking effects of ferromagnetic exchange splitting, and hence to the thickness of the magnetic layers, temperature, and magnetic scattering impurities. The amplitudes of the opposite-spin correlations pervading the adjacent ferromagnet, undergo damped oscillations as a function of position which reveals itself in $0-\pi$ transitions of the supercurrent.^{1,7-10} Since about a decade ago, several proposals have been put forth to achieve attainable and practical platforms that isolate and utilize the proximity-induced^{3,4} superconducting triplet correlations in *SF* hybrids.^{1,2}

The signatures of the proximity-induced electronic density of states (DOS) in the *F* layers of these hybrid structures can reveal the existence and type of superconducting correlations in the region.⁹⁻¹³ One promising prospect for unambiguously detecting triplet correlations experimentally involves tunneling spectroscopy experiments which can probe the local single particle spectra encompassing the proximity-induced DOS.^{11,12,14-29} Nonetheless, competing effects can make analysis of the results of such a ‘direct’ probe of spin-

triplet superconducting correlations problematic. The DOS in *SNS* junctions and *SFS* heterostructures where the magnetization pattern of the *F* layer can be either uniform or textured (including domain wall and nonuniform textures, such as the spiral magnetic structure of Holmium) has been extensively studied.^{11,12,20-22,30,31} It was found that the DOS in a normal metal sandwiched between two *s*-wave superconducting banks shows a minigap which closes by simply tuning the superconducting phase differences up to the value of π .^{11,12,21,22} In contrast, the DOS can exhibit anomalous behavior in inhomogeneous magnetic layers. Namely, upon modulating the superconducting phase difference^{11,12} a peak arises at zero energy, at the center of what was a minigap. It was also shown that the zero energy peak (ZEP) in the DOS for a simple textured *SFS* junction can be maximized at a π bias.^{11,12} The minigap-to-peak behavior of the DOS at zero energy is an important signature of the emergence of triplet correlations.^{11,12} Recently it was theoretically proposed that the minigap-to-peak phenomenon be leveraged for functionality in device platforms such as SQUIDs, to enhance their performance and as ultrasensitive switching devices, including a *singlet-triplet* superconducting quantum magnetometer.²³

An important spectroscopic tool for investigating proximity effects on an atomic scale with sub-meV energy resolution is the scanning tunneling microscope (STM). As shown in Fig. 1, an *SFF* spin valve structure can be probed experimentally by positioning a nonmagnetic STM tip at the edge of the sample to measure the tunneling current (*I*) and voltage (*V*) characteristics. This technique yields a direct probe of the available electronic states with energy *eV* near the tip. Therefore, the differential conductance $dI(V)/dV$ over the energy range of interest is proportional to the local DOS. Numerous experiments have reported signatures of the energy spectra in this manner.^{14,15,17-19,24-26,28} When ferromagnetic elements are present, the superconducting proximity-induced DOS reveals a number of peculiarities due to the additional spin degree of freedom that arises from the magnetic layers. However, the experimental signatures of the odd-frequency spin-triplet correlations can be washed out by more dominate

singlet correlations. When the exchange splitting h of the magnetic layers is large ($\sim \varepsilon_F$, i.e. close to the half metallic limit), the characteristic length scale ξ_F that describes the propagation length of opposite-spin pairs in the ferromagnets is extremely small. These types of proximity-induced correlations can thus only be experimentally observed in weak magnetic alloys $h \ll \varepsilon_F$ (such as Cu_xNi_y) or thin F layers so that d_F/ξ_F is sufficiently large to allow the opposite-spin superconducting correlations to propagate in the ferromagnet without being completely suppressed.^{14,16,27} Since spin-1 triplet pairs are not destroyed by the ferromagnetic exchange field in strong magnets, there should exist certain system parameters, e.g., ferromagnet widths and exchange fields, that result in regions whereby equal-spin pairs are the only pair correlations present. This scenario was explored in a S/Ho bilayer²⁹, where phase-periodic conductance oscillations were observed in Ho wires connected to an ordinary s-wave superconductor. This behavior was qualitatively explained in terms of the long-range penetration of proximity-induced spin-1 triplet pairings due to the helical structure of the magnetization.³² In practice however, simpler structures involving SF hybrids with uniform exchange fields are often preferable from both an experimental and theoretical perspective.^{14,16,17,24-29} Therefore, the primary aim of this work is the determination of experimentally optimal parameters for probing odd-frequency spin-1 triplet correlations with DOS signatures in nanoscale SFF spin valves.

Nearly all of the past theoretical works on SFF structures have considered the diffusive case,³³⁻³⁵ where impurities strongly scatter the quasiparticles. The clean regime has been studied, using a self-consistent solution of the Bogoliubov-de Gennes (BdG)³⁶ equations, in Ref. 37. That work, however, focused largely on the transition temperature oscillations. The results for these oscillations were found³⁸ to agree with experiment and to be consistent with other experimentally established³⁹⁻⁴² results. In the present work, we use the same general methods used there to study a simple SFF structure with noncollinear exchange fields in the ballistic regime, but we focus on a very different quantity which is readily accessible experimentally, namely the local DOS and its detailed low-energy structure. We strongly emphasize the relation between the ZEP and the triplet pairing amplitudes. In particular, given the assertion³⁸ that variations in the transition temperature in these valve structures are quantitatively related to the average triplet pair amplitudes in the outer F layer, we will search for, (and, as will be seen, find) correlations between the ZEP and these averages. This BdG study is complemented with a briefer investigation of the corresponding diffusive case. By considering both regimes, we will be able to provide some general guidelines for future experiments.

The structure we study is schematically depicted in Fig. 1, where the STM tip is positioned at the outermost F layer, near the vacuum boundary. In the ballistic regime, we employ the full microscopic BdG equations within a self-consistent framework. From the solutions, we calculate the local DOS over a broad range of experimentally relevant parameters, and study its behavior at low energies. For the diffusive regime, we make use of the quasiclassical Usadel⁴³ approach to study

the diffusive SFF counterparts in the full proximity limit. Our systematic investigations thus provide a comprehensive guide into such spin valves. Utilizing experimentally realistic parameters, we determine favorable thicknesses for the F layers to induce maximal ZEPs, which occurs when the population of triplet correlations in the outer layer, dominates the singlets.

The paper is organized as follows. In Sec. II we outline the theoretical approaches used. In Sec. III, we present our results in two subsections, pertaining to the ballistic and diffusive regimes. In the ballistic case, we study the local DOS for differing exchange field misalignments, exchange field intensities, and interface scattering strengths. We also investigate the singlet and triplet pairing correlations for similar parameters to determine how ZEPs in the DOS correlate with the triplet correlations. In the diffusive case, we present two-dimensional maps of the ZEP at different exchange field misalignments, and SF interface opacity. Finally, we summarize with concluding remarks in Sec. IV.

II. METHODS AND THEORETICAL TECHNIQUES

In this section, we first discuss the theoretical framework used to study clean samples. We then outline the Usadel technique in the full proximity regime, which properly describes dirty samples.

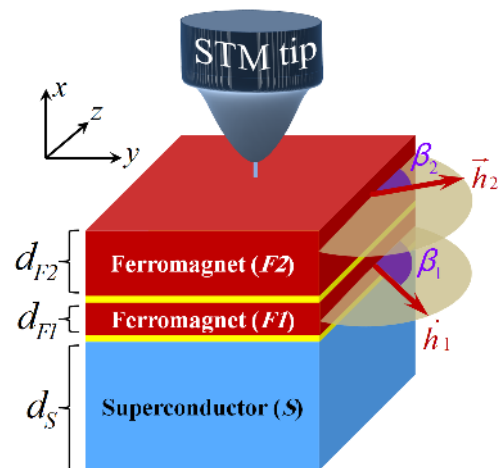


FIG. 1. (Color online) Schematic of the SFF spin-valve structure. The ferromagnetic layers have uniform exchange fields located in the yz plane. The exchange field of each layer is defined by $\vec{h}_{1,2} = h_0(0, \sin \beta_{1,2}, \cos \beta_{1,2})$ in which $\beta_{1,2}$ are the angle of the exchange fields with respect to the z direction. The ferromagnets (F_1 , F_2) and superconductor (S) are stacked in the x direction with thickness d_{F1} , d_{F2} , and d_S , respectively. The STM tip is located at edge of the SFF spin-valve.

A. Microscopic approach: Bogoliubov-de Gennes equation

For the ballistic regime, we use the microscopic BdG equations to study SFF spin valve nanostructures. We solve these equations in a fully self-consistent^{37,44} manner. A schematic of the spin valve configuration is depicted in Fig. 1. The general spin-dependent BdG equations for the quasiparticle energies, ϵ_n , and quasiparticle amplitudes, $u_{n\sigma}$, $v_{n\sigma}$ is written:

$$\begin{pmatrix} H_0 - h_z & -h_x + ih_y & 0 & \Delta \\ -h_x - ih_y & H_0 + h_z & \Delta & 0 \\ 0 & \Delta^* & -(H_0 - h_z) & -h_x - ih_y \\ \Delta^* & 0 & -h_x + ih_y & -(H_0 + h_z) \end{pmatrix} \begin{pmatrix} u_{n\uparrow} \\ u_{n\downarrow} \\ v_{n\uparrow} \\ v_{n\downarrow} \end{pmatrix} = \epsilon_n \begin{pmatrix} u_{n\uparrow} \\ u_{n\downarrow} \\ v_{n\uparrow} \\ v_{n\downarrow} \end{pmatrix}, \quad (1)$$

where the pair potential, $\Delta(x)$, is calculated self-consistently as explained below. This quasi one-dimensional system is described by the single particle Hamiltonian $\mathcal{H}_0(x)$ as,

$$\mathcal{H}_0(x) \equiv \frac{1}{2m} (-\partial_x^2 + k_y^2 + k_z^2) - E_F + U(x), \quad (2)$$

where E_F is the Fermi energy, and $U(x)$ is the spin-independent interface scattering potential which we take to be of the form $U(x) = H[\delta(x - d_{F1}) + \delta(x - d_{F1} - d_{F2})]$. The in-plane wavevector components, k_y and k_z , arise from the translational invariance in the y and z directions. The system is finite in the x direction, with widths of each F and S layer shown in the schematic. Our method permits arbitrary orientations and magnitudes of the magnetic exchange fields, \vec{h}_i ($i = 1, 2$), in each of the ferromagnet regions. Specifically, we fix the exchange field in F_2 to be aligned in the z direction, while in F_1 , its orientation is described by the angle β_1 :

$$\vec{h} = \begin{cases} \vec{h}_1 = h_0(0, \sin \beta_1, \cos \beta_1), & \text{in } F_1 \\ \vec{h}_2 = h_0 \hat{z}, & \text{in } F_2, \end{cases} \quad (3)$$

where we consider the experimentally appropriate situation of an in-plane Stoner-type exchange field interaction.

The spin-splitting effects of the exchange field coupled with the pairing interaction in the S regions, results in a nontrivial spatial dependence of the pair potential $\Delta(x)$. In general, it is necessary to calculate the pair potential in a self consistent manner by an appropriate sum over states:

$$\Delta(x) = \frac{g(x)}{2} \sum_n [u_{n\uparrow}(x)v_{n\downarrow}^*(x) + u_{n\downarrow}(x)v_{n\uparrow}^*(x)] \tanh\left(\frac{\epsilon_n}{2T}\right), \quad (4)$$

where $g(x)$ is the attractive interaction that exists solely inside the superconducting region and the sum is restricted to those quantum states with positive energies below an energy cutoff, ω_D .

We now discuss the appropriate quantities that characterize the induced triplet correlations. We define^{4,45} the following

triplet pair amplitude functions in terms of the field operators in the Heisenberg picture,

$$f_0(x, t) = \frac{1}{2} [\langle \psi_\uparrow(x, t) \psi_\downarrow(x, 0) \rangle + \langle \psi_\downarrow(x, t) \psi_\uparrow(x, 0) \rangle], \quad (5a)$$

$$f_1(x, t) = \frac{1}{2} [\langle \psi_\uparrow(x, t) \psi_\uparrow(x, 0) \rangle - \langle \psi_\downarrow(x, t) \psi_\downarrow(x, 0) \rangle], \quad (5b)$$

where t is the relative time. With the quantization axis aligned along the z direction, the time-dependent triplet amplitudes, $f_0(x, t)$ and $f_1(x, t)$, can be written in terms of the quasiparticle amplitudes:^{4,45}

$$f_0(x, t) = \frac{1}{2} \sum_n (f_n^{\uparrow\downarrow}(x) - f_n^{\downarrow\uparrow}(x)) \zeta_n(t), \quad (6)$$

$$f_1(x, t) = \frac{1}{2} \sum_n (f_n^{\uparrow\uparrow}(x) + f_n^{\downarrow\downarrow}(x)) \zeta_n(t), \quad (7)$$

where we define $f_n^{\sigma\sigma'}(x) = u_{n\sigma}(x)v_{n\sigma'}^*(x)$, and the time factor $\zeta_n(t)$ is written,

$$\zeta_n(t) = \cos(\epsilon_n t) - i \sin(\epsilon_n t) \tanh\left(\frac{\epsilon_n}{2T}\right). \quad (8)$$

Experimentally accessible information regarding the quasiparticle spectra is contained in the local density of one particle excitations in the system. This includes the zero-energy signatures in the density of states (DOS), which present a possible experimental avenue in which to detect the emergence of equal-spin triplet correlations within the outer ferromagnet. The total DOS, $N(x, \epsilon)$, is the sum $N_\uparrow(x, \epsilon) + N_\downarrow(x, \epsilon)$, involving the spin-resolved local density of states (DOS), N_σ , which are written,

$$N_\sigma(x, \epsilon) = - \sum_n \left\{ [u_n^\sigma(x)]^2 f'(\epsilon - \epsilon_n) + [v_n^\sigma(x)]^2 f'(\epsilon + \epsilon_n) \right\}, \quad (9)$$

where σ denotes the spin ($=\uparrow, \downarrow$), and $f'(\epsilon) = \partial f / \partial \epsilon$ is the derivative of the Fermi function.

B. Quasiclassical approach: Usadel equation

When the system contains a strong impurity concentration, then for sufficiently small energy scales, the superconducting correlations are governed by the Usadel equation. Following Ref. 12, the Usadel equation⁴³ compactly reads:

$$\mathcal{D} \left[\partial, G(\mathbf{r}, \epsilon) \left[\partial, G(\mathbf{r}, \epsilon) \right] \right] + i \left[\epsilon \rho_3 + \text{diag} [\mathbf{h}(\mathbf{r}) \cdot \boldsymbol{\sigma}, (\mathbf{h}(\mathbf{r}) \cdot \boldsymbol{\sigma})^T], G(\mathbf{r}, \epsilon) \right] = 0, \quad (10)$$

in which ρ_3 and $\boldsymbol{\sigma} = (\sigma^x, \sigma^y, \sigma^z)$ are 4×4 and 2×2 Pauli matrices, respectively, and \mathcal{D} represents the diffusive constant of the magnetic region. The quasiclassical approach employed in this section supports ferromagnets with arbitrary exchange field directions; $\mathbf{h}(\mathbf{r}) = (h^x(\mathbf{r}), h^y(\mathbf{r}), h^z(\mathbf{r}))$. In Eq. (10),

G represents the total Green's function which is made of Advanced (A), Retarded (R), and Keldysh (K) blocks. Therefore, the total Green's function can be expressed by:

$$G(\mathbf{r}, \epsilon) = \begin{pmatrix} G^R & G^K \\ 0 & G^A \end{pmatrix}, \quad G^R(\mathbf{r}, \epsilon) = \begin{pmatrix} \mathcal{G} & \mathcal{F} \\ -\mathcal{F}^* & -\mathcal{G}^* \end{pmatrix}. \quad (11)$$

In the presence of ferromagnetism, the components of advanced block, $G^A(\mathbf{r})$, of total Green's function G can be written as:

$$\mathcal{F}(\mathbf{r}, \epsilon) = \begin{pmatrix} f_{\uparrow\uparrow} & f_{\uparrow\downarrow} \\ f_{\downarrow\uparrow} & f_{\downarrow\downarrow} \end{pmatrix}, \quad \mathcal{G}(\mathbf{r}, \epsilon) = \begin{pmatrix} g_{\uparrow\uparrow} & g_{\uparrow\downarrow} \\ g_{\downarrow\uparrow} & g_{\downarrow\downarrow} \end{pmatrix}. \quad (12)$$

In this paper, however, we assume stationary conditions for our systems under consideration, and hence the three blocks comprising the total Green's function are related to each other in the following way: $G^A(\mathbf{r}, \epsilon) = -[\rho_3 G^R(\mathbf{r}, \epsilon) \rho_3]^\dagger$, and $G^K(\mathbf{r}, \epsilon) = \tanh(\beta\epsilon)[G^R(\mathbf{r}, \epsilon) - G^A(\mathbf{r}, \epsilon)]$, where $\beta \equiv k_B T/2$.

The SF interface controls the proximity effect. Therefore, appropriate boundary conditions should be considered to properly model the system. In our work, we consider the Kupriyanov-Lukichev boundary conditions at the SF interface⁴⁶ which controls the induced proximity correlations using a parameter ζ as the barrier resistance:

$$\zeta G(\mathbf{r}, \epsilon) \partial G(\mathbf{r}, \epsilon) = [G_{\text{BCS}}(\theta, \epsilon), G(\mathbf{r}, \epsilon)]. \quad (13)$$

The solution for a bulk even-frequency s -wave superconductor G_{BCS}^R reads,³²

$$\hat{G}_{\text{BCS}}^R(\theta, \epsilon) = \begin{pmatrix} \mathbf{1} \cosh \vartheta(\epsilon) & i\sigma^y \sinh \vartheta(\epsilon) \\ i\sigma^y \sinh \vartheta(\epsilon) & -\mathbf{1} \cosh \vartheta(\epsilon) \end{pmatrix}, \quad (14)$$

where $\vartheta(\epsilon) = \text{arctanh}(|\Delta|/|\epsilon|)$.

The system local density of states, $\mathcal{N}(\mathbf{r}, \epsilon)$, can be expressed by the following equation:

$$\mathcal{N}(\mathbf{r}, \epsilon) = \frac{\mathcal{N}_0}{2} \text{Re} \left[\text{Tr} \{ G(\mathbf{r}, \epsilon) \} \right], \quad (15)$$

in which \mathcal{N}_0 is the density of state normal state.

III. RESULTS AND DISCUSSION

In this section, we describe our results. We start with those for a ballistic SFF structure and then present the predictions of Usadel formalism for diffusive samples.

A. Ballistic Regime

In this subsection we present the self-consistent results for the ballistic regime. The numerical method used here to iteratively solve in a self consistent way Eqs. (1) and (4) has been extensively described elsewhere,^{37,44} and details need not be repeated here. In the calculations, the temperature

T is held constant at $T = 0.05T_c$, where T_c is the transition temperature of a pure bulk S sample. All length scales are normalized by the Fermi wavevector, so that the coordinate x is written $X = k_F x$, and the F_1 and F_2 widths are written $D_{Fi} \equiv k_F d_{Fi}$, for $i = 1, 2$. The ferromagnet F_2 and superconductor are set to fixed values, corresponding to $D_{F2} = 400$, and $D_S = 600$, respectively. We also assume a coherence length corresponding to $k_F \xi_0 = 100$. One of our main objectives in this paper is to study the triplet correlations, which are odd in time.⁴ To accomplish this, we employ the expressions in Eqs. (6) and (7), which describe the spatial and temporal behavior of the triplet amplitudes. At $t = 0$ the triplet correlations vanish because of the Pauli exclusion principle. At finite t , the triplet correlations generated near the S/F interface tend to increase in amplitude and spread throughout the structure. We normalize the time t according to $\tau = \omega_D t$, and we set it to a representative³⁷ value of $\tau = 4$. We can then study the behavior of the triplet amplitudes f_0 and f_1 throughout the junction. To explore the proximity induced signatures in the single-particle states, which is the main purpose of this work, we then present a systematic investigation of the experimentally relevant local DOS. All DOS results presented are local values taken at a fixed position near the edge of the sample in the F_2 region. We characterize interface scattering, when present, by delta functions of strength H , which we write in terms of the dimensionless parameter $H_B \equiv H/v_F$. Finally, we use natural units, e.g., $\hbar = k_B = 1$ throughout.

Triplet and singlet pair correlations

Here we present results for both the triplet and singlet correlations, calculated using Eqs. (6)-(7). For the cases shown below, the absolute value of the singlet and triplet complex quantities are averaged over the region of interest, which in this case is the experimentally probed F_2 region. An important reason for focusing on those spatially averaged (over the outer magnet) quantities, rather than the spatial profiles discussed in Ref. 37, is that it was experimentally shown³⁸ that these triplet averages perfectly anticorrelate with the transition temperatures, i.e. the spin valve effect. We also normalize all pair correlations to the value of the bulk singlet pair amplitude. We begin by showing, in Fig. 2, the spatially averaged absolute value of the complex triplet amplitudes $|f_{0,\text{avg}}|$ (with spin projection $m = 0$), and $|f_{1,\text{avg}}|$ (with spin projection $m = \pm 1$) along with the singlet $|f_{3,\text{avg}}|$, (note that $f_3(x) \equiv \Delta(x)/g(x)$) as functions of D_{F1} . Each row of panels corresponds to a different exchange field value: from top to bottom rows, we have $h/\varepsilon_F = 0.5, 0.1$, and 0.05 . Examining the opposite spin correlations, f_0 and f_3 , damped oscillatory behavior with D_{F1} is evident: this is related to the spatial oscillation of the Cooper pairs due to their acquiring a center of mass momentum when entering the magnet.⁴⁷ Therefore, the wavelength of these oscillations varies inversely with the exchange field in F_2 (this is why the D_{F1} range for the weaker exchange fields is extended). Quantum interference effects generate peaks in f_0 and f_3 that occur approximately when

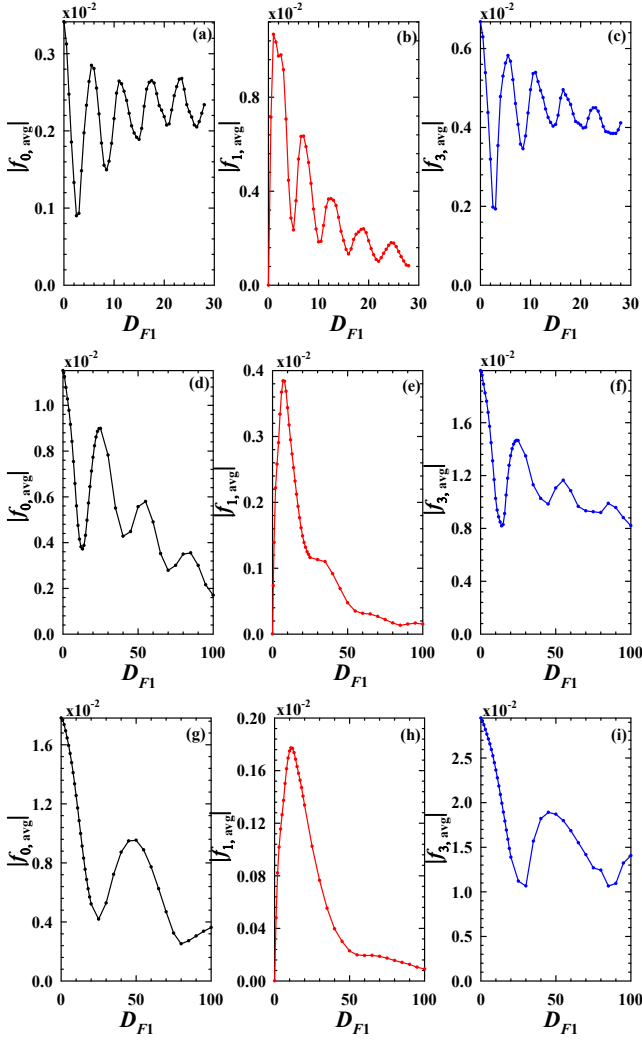


FIG. 2. (Color online) The absolute value of the normalized triplet and singlet pair correlations, averaged over the F_2 region, as a function of D_{F1} . The exchange field strengths are (from top to bottom): $h/\epsilon_F = 0.5, 0.1, 0.05$. The relative exchange field orientations are orthogonal, with $\beta_1 = \pi/2$, and $\beta_2 = 0$.

$d_{F1}/\xi_F = n\pi$, (i.e. $D_{F1} = n\pi(h/\epsilon_F)^{-1}$). In the ballistic regime, the length scale that characterizes the damped oscillations is $\xi_F = v_F/(2h)$, where v_F is the Fermi velocity. The equal-spin amplitudes f_1 , are seen to behave oppositely, with a phase offset of approximately $\pi/2$. Their magnitude declines more rapidly with D_{F1} , compared to the behaviors of f_0 and f_3 . This is consistent with f_1 triplet generation being optimal for highly asymmetric ferromagnetic layer widths.³² It is notable that the periodic occurrence of peaks in f_1 when varying D_{F1} , evolves into a single maximum as h is reduced further.

One of the strengths of the microscopic BdG formalism is having the ability to properly include the full microscopic range of length and energy scales inherent to the problem. This includes the exchange energy h , which in our BdG framework can span the limits from a nonmagnetic normal

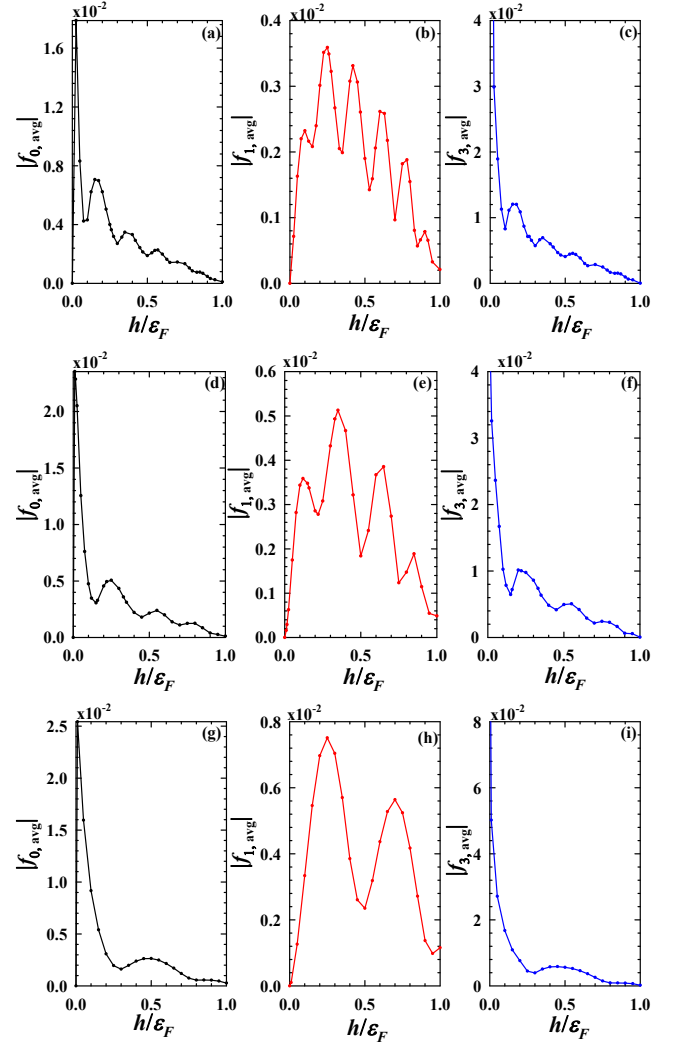


FIG. 3. (Color online) The spatially averaged (in F_2) normalized triplet and singlet pair correlations as a function of h/ϵ_F . As in Fig. 2, the magnitude of each quantity is taken and averaged over the F_2 region. Each row of panels corresponds to a different F_1 width, with $D_{F1} = 15$ (top row), $D_{F1} = 10$ (middle row), and $D_{F1} = 5$ (bottom row). The relative exchange field orientations are orthogonal, with $\beta_1 = \pi/2$, and $\beta_2 = 0$.

metal ($h/\epsilon_F = 0$) to a half-metallic ferromagnet ($h/\epsilon_F = 1$). It is particularly useful to consider the behavior of the singlet and triplet correlations over this broad range of strengths of h/ϵ_F . Thus, in Fig. 3, we show the same quantities as Fig. 2, plotted now as a function h/ϵ_F . Again, we have orthogonal relative exchange field orientations, with $\beta_1 = \pi/2$, and $\beta_2 = 0$. Each three-panel row corresponds to a different F_1 width: $D_{F1} = 15, 10$, and 5 (from top to bottom). The central column reveals that the averaged equal spin amplitudes $|f_{1,avg}|$ displays regularly occurring prominent peaks, the number of which varies with the length of the F_1 region. For the exchange fields and F_1 widths considered in Fig. 2, the triplet f_1 was generally weaker than either the singlet f_3 or triplet f_0 . For the system parameters used in Fig. 3 how-

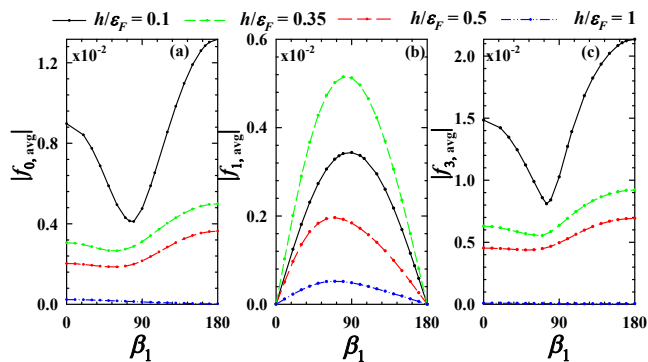


FIG. 4. (Color online) Plots of the averaged singlet and triplet components as a function of magnetic orientation β_1 . Here $D_{F1} = 10$, and results for several magnetic strengths are shown, ranging from weak to half-metallic.

ever, we find that for narrow widths D_{F1} and sufficiently large exchange fields, the equal-spin triplet component f_1 can dominate the other pair correlations. In particular, for strong ferromagnets with $h/\varepsilon_F \approx 0.8$, and thin F_1 layers with $D_{F1} = 5$, panels (g) and (i) illustrate that the f_0 and f_3 amplitudes consisting of opposite spin pairs, are negligible due to the pair breaking effects of the strong magnet. On the other hand, the equal-spin pairs shown in panel (h) are seen to survive in this limit. This has important consequences for isolating and measuring this triplet component in experiments.

Having seen how the magnitude of the exchange field h affects the singlet and triplet correlations, we next investigate the effects of changing its direction. Therefore, we examine in Fig. 4, the behavior of the averaged singlet and triplet amplitudes when changing the magnetic orientation angle, β_1 . We again consider a broad range of exchange field strengths, as shown in the legend. One of the more obvious features is that the maximum of $|f_{1, \text{avg}}|$ typically does not occur for orthogonal relative exchange fields,³⁵ for smaller $\beta_1 \lesssim 90^\circ$, especially for stronger magnets. This is in agreement with previous^{34,35,37,38,48-50} experimental and theoretical results. Due to the non-monotonicity of $|f_{1, \text{avg}}|$ with h [see Fig. 3(e)], the $h/\varepsilon_F = 0.35$ case seen in Fig. 4(b) is larger for all β_1 than for the weaker $h/\varepsilon_F = 0.1$ case. The singlet f_3 and triplet f_0 amplitudes are largest for antiparallel configurations ($\beta_1 = 180^\circ$), where the opposite exchange fields are effectively weakened, with reduced spin-splitting effects on the opposite-spin Cooper pairs. This is a well-known result. The results also show that the relative magnetic orientation angles leading to the minima of these two quantities are anticorrelated with the angles at which the f_1 correlations are maximal. As seen in Figs. 4(a) and (c), $|f_{0, \text{avg}}|$ and $|f_{3, \text{avg}}|$ decay much more abruptly as the value of h in the magnets approaches the half-metallic limit: this is consistent with the discussions above. Therefore, SFF structures involving strong ferromagnets ($h \sim \varepsilon_F$) with β_1 at or near orthogonal orientations, can host larger generated triplet pair correlations whereby $|f_1| \gg \{|f_0|, |f_3|\}$, thus allowing for direct probing of the spin triplet superconducting correlations in experiments.

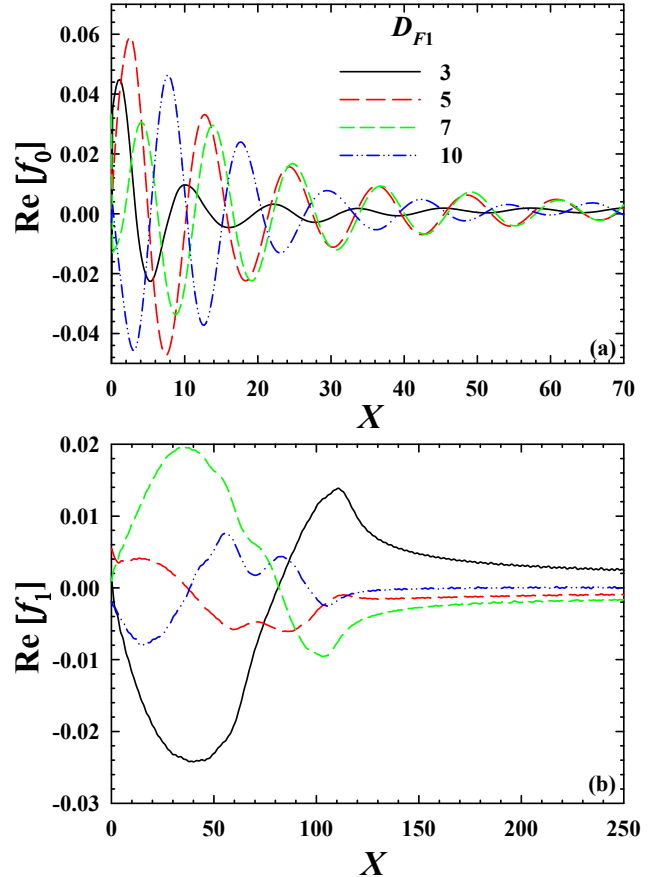


FIG. 5. (Color online) Local spatial profiles of the real parts of the triplet components f_0 and f_1 in the F_2 region for a few different F_1 widths, D_{F1} . The exchange field in the ferromagnets corresponds to $h/\varepsilon_F = 0.5$, and the relative exchange field orientations are orthogonal, with $\beta_1 = \pi/2$, and $\beta_2 = 0$.

More detailed information regarding the triplet amplitudes, can be obtained from the spatial profiles of the local triplet correlations within the F_2 region. In Fig. 5, we present the real parts of the normalized $f_0(x)$ and $f_1(x)$ triplet components in terms of the dimensionless coordinate X . Results are plotted at four different values of D_{F1} as indicated in the legend. The exchange fields in the ferromagnets has magnitude corresponding to $h/\varepsilon_F = 0.5$, and the directions are mutually orthogonal, with $\beta_1 = 90^\circ$, and $\beta_2 = 0$. For the time scale considered here, the imaginary part of f_0 is typically much smaller than its real part. As to f_1 , its imaginary part is usually not negligible, but it exhibits trends that are similar to those for the real part. Examining the top panel, it is evident that f_0 exhibits the trademark damped oscillatory spatial dependence arising from the difference in the spin-up and spin-down wavevectors of the Cooper pairs. The oscillatory wavelength is thus governed by the quantity $2\pi k_F \xi_F = 2\pi(h/\varepsilon_F)^{-1}$, which for our parameters corresponds to 4π . The modulating f_0 has the same wavelength for each D_{F1} , although each curve can differ in phase. The averaged f_0 amplitudes are con-

sistent with this local behavior: Fig. 2(a) demonstrated that when $D_{F1} \approx 5$ and $D_{F1} \approx 10$, there is an enhancement of the f_0 component, while for $D_{F1} \approx 3$, it is substantially reduced. The equal-spin f_1 amplitudes, are shown in the bottom panel of Fig. 5. Near the interface at $X = 0$, the f_1 correlations are created, and then they subsequently increase in magnitude until deeper within the ferromagnet, where they clearly exhibit a gradual long-ranged decay. The trends observed here are opposite to those in the top panel, where for instance the $D_{F1} = 3$ case leads to maximal f_1 triplet generation, in agreement with Fig. 2(b).

Local density of states

After the discussion of the salient features of the singlet and triplet pair correlations in the outer F layer, we now turn to the main topic of the paper: the local density of states measured in F_2 . This is the experimentally relevant quantity that can reveal the signatures of these correlations. The damped oscillatory behavior of the pair correlations can lead to spectroscopic signatures in the form of DOS inversions,⁵¹ and multiple oscillations.²⁴ In the quasiclassical approximation,^{34,35,48,49} a ZEP can emerge from the long-range triplet correlations^{32,52} in SFF systems. However, this approximation is not appropriate for experimental conditions involving strong magnets and clean interfaces. It would be beneficial experimentally to characterize the ZEP relation to the singlet and triplet correlations and see how the ZEP may be a useful fingerprint in identifying the existence of the long-range triplet component. To properly do this over the broad range of parameters found in experimental conditions, a microscopic self-consistent theory that can accommodate the wide ranging length and energy scales is needed. In this subsection, we therefore present an extensive microscopic study of the ZEP as a function of parameters such as F layer thicknesses, exchange energy, or interface transparency. These results are then correlated with the self-consistent singlet and triplet pair correlations in the previous subsection. In what follows, the DOS is normalized by the DOS at the Fermi level \mathcal{N}_F , and plotted vs the normalized energy ε/Δ_0 , where Δ_0 is the bulk value of the pure S material gap at zero temperature. Our emphasis will be on energies within the subgap region $\varepsilon \leq \Delta_0$, where the ZEP phenomenon arises. Since the DOS is a local quantity that depends on position [see Eq. (9)], in our calculations we assume the location to be near the edge of the sample just below the STM tip as shown in Fig. 1.

To correlate the triplet correlations in Fig. 3 with the ZEP, we begin by studying in Fig. 6 the sensitivity of the DOS to a broad range of exchange field strengths h . Each panel corresponds to a different F_1 width, D_{F1} . The range of h considered in each panel varies since the largest ZEP depends on the relative values of h and D_{F1} . The top panel ($D_{F1} = 5$) clearly shows the progression of the ZEP with h : Beginning with the smallest exchange field, $h/\varepsilon_F = 0.1$, a moderate peak is observed that increases to its maximum height and narrower width when $h/\varepsilon_F = 0.2$. Further increases in h continuously diminish the ZEP, broadening its width, until eventu-

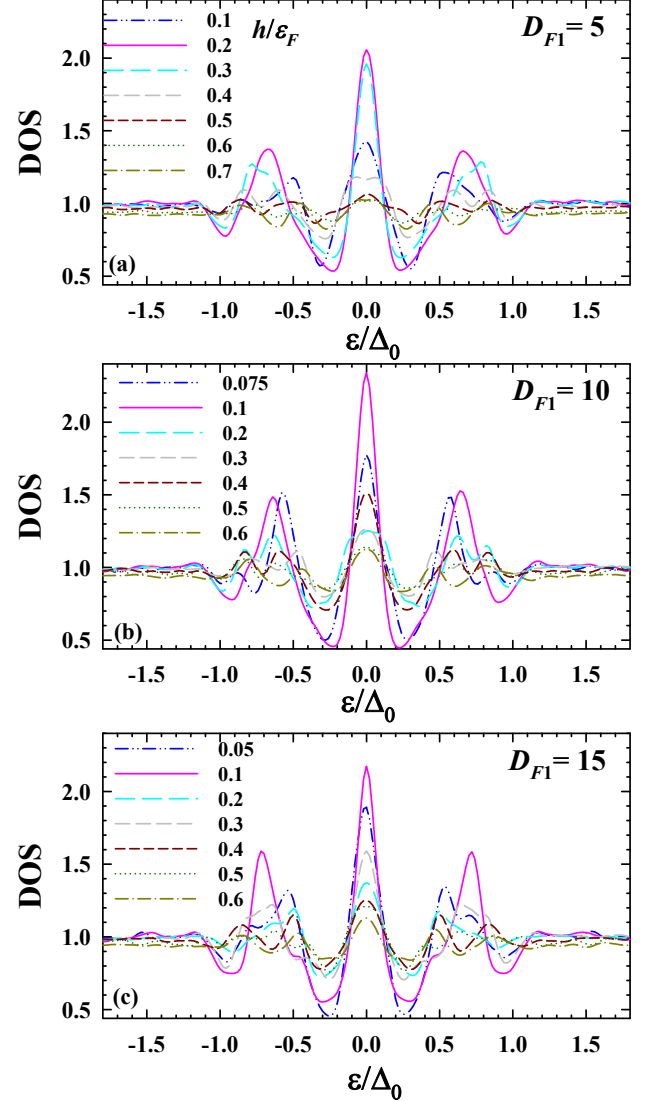


FIG. 6. (Color online) Normalized (see text) local DOS. The multiple curves in each panel are for different values of h/ε_F . Each panel corresponds to a different value of D_{F1} (as labeled). The ferromagnets have exchange fields with orthogonal relative directions.

ally it is effectively washed away. This non-monotonic behavior is consistent with the ZEP being related to the presence of the f_1 triplet amplitude near the edge of the ferromagnet. This can be seen by reexamining the triplet amplitudes in Fig. 3(h), where the exchange field leading to the highest ZEP occurs when $|f_{1,\text{avg}}|$ is largest, at $h/\varepsilon_F \approx 0.2$. The same consistency is found between Figs. 2(e) and (b) and the middle and lower panels of Fig. 3, respectively. For both the $D_{F1} = 10, 15$ cases, the average value of $|f_1|$ is largest near $h/\varepsilon_F = 0.1$. However, the secondary peak structure in Fig. 2 is not clearly reflected in the DOS.

Next we study the DOS counterpart to Fig. 2. The normalized DOS, and the corresponding ZEP, are shown in Fig. 7 for

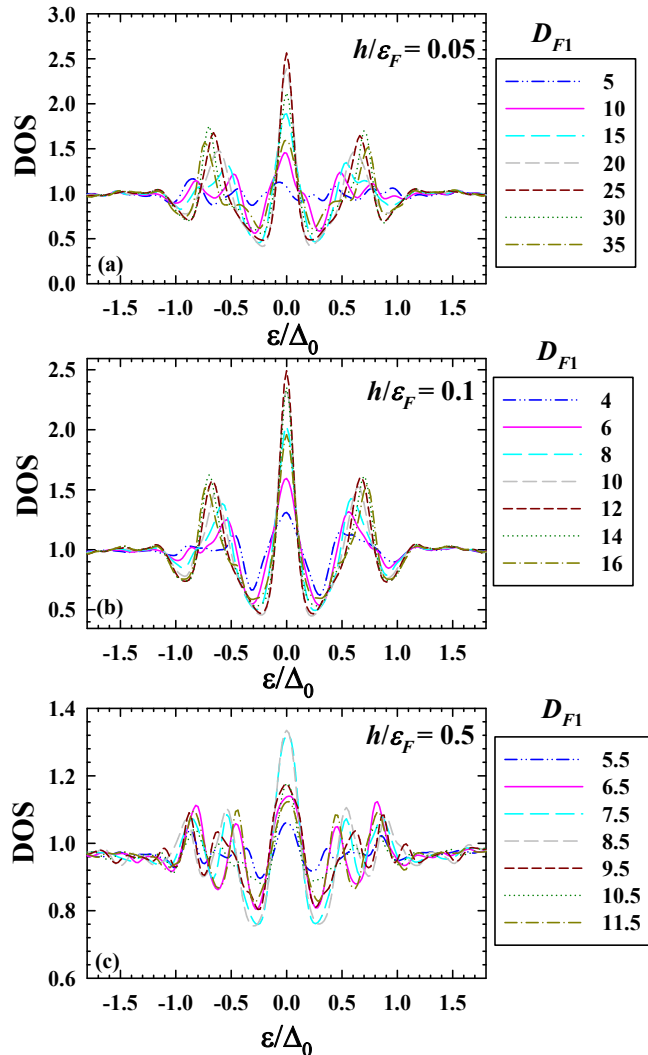


FIG. 7. (Color online) Normalized local DOS as a function of the normalized energy. The curves in each panel are for different values of the width D_{F1} . Each panel corresponds to a different h/ϵ_F : $h/\epsilon_F = 0.05, 0.1, 0.5$, and we consider orthogonal relative exchange fields.

a broad range of widths D_{F1} . The parameter values here are similar to those used in Fig. 2, where each panel corresponds to a different exchange field. In panel (a) with $h/\epsilon_F = 0.05$, the most prominent ZEP occurs for $D_{F1} = 25$, coinciding with the F_1 width that yields a local maximum for the $m = 0$ triplet amplitude f_0 (see Fig. 2(g)). By comparison, the f_1 component observed in Fig. 2(h), is smaller and lacks the multiple peak structure found for f_0 , at this weaker exchange field. Therefore, the largest ZEP in the case of weak exchange fields, does not necessarily occur when the triplet f_1 is maximal; as Fig. 2(h) demonstrated, $|f_{1,\text{avg}}|$ peaks at $D_{F1} = 10$ before rapidly declining. For these weaker fields, it follows from Fig. 2 that the magnitude of f_0 exceeds that of f_1 . It would appear then that it is the larger triplet component which de-

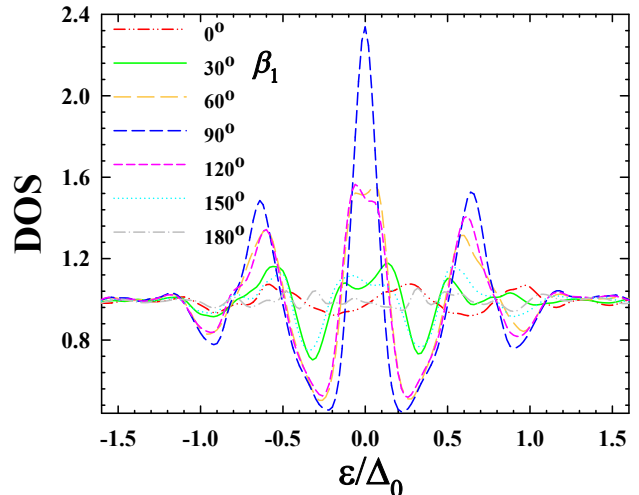


FIG. 8. (Color online) Variation of the normalized local DOS with the in-plane exchange field angle β_1 . The exchange field is fixed along z in F_2 . Also, $D_{F1} = 10$, and $h/\epsilon_F = 0.1$.

termines the ZEP structure. This is consistent with the known result³⁸ that the *total* value of the triplet component is correlated with T_c . The next case in panel (b) corresponds also to a moderately weak magnet with $h/\epsilon_F = 0.1$, or double the exchange field considered in panel (a). Since the frequency of the oscillations involving the opposite-spin f_0 amplitudes [see Fig. 2(d)] also doubles, the maximum ZEP at $D_{F1} = 12$, occurs at about half the F_1 width found for the maximum ZEP in (a). The equal-spin triplet correlations f_1 were seen in Fig. 2(e) to exhibit a single peak structure, but their magnitude is larger than at weaker fields. This is because typically stronger magnets in this situation lead to an enhancement of the f_1 amplitudes. Lastly, we consider (bottom panel) a relatively strong ferromagnet with $h/\epsilon_F = 0.5$. For this case, there are additional subgap peaks flanking the main ZEP. The larger ZEP arises at smaller widths ($D_{F1} = 7.5, 8.5$) than for weaker exchange fields, due to an increase in the frequency of the oscillations as a function of D_{F1} for the f_0 and f_1 components as seen in Fig. 2(a) and (b). Thus, the ZEP tends to exhibit a structure that dampens and widens for strong magnets, while the opposite is true for weaker ones and is correlated with the stronger of the $m = 0$ and $m = \pm 1$ triplet components present.

Having established the behavior of the ZEP for differing h/ϵ_F , we now fix the magnitude of the exchange fields in each magnet and investigate the effects of varying their relative orientation. Figure 8 illustrates the normalized DOS for the specific case $D_{F1} = 10$, and $h/\epsilon_F = 0.1$. According to Fig. 4(b), the equal-spin triplet component f_1 is greatest when $\beta_1 \approx 90^\circ$. Thus we would expect the ZEP to also be maximal at this angle. Figure 8 shows that this is indeed the case. There the normalized DOS is shown for a range of $0^\circ \leq \beta_1 \leq 180^\circ$ in increments of 30° . Clearly the orthogonal relative exchange field ($\beta_1 = 90^\circ$) configuration results in the most prominent ZEP. When β_1 deviates from this angle

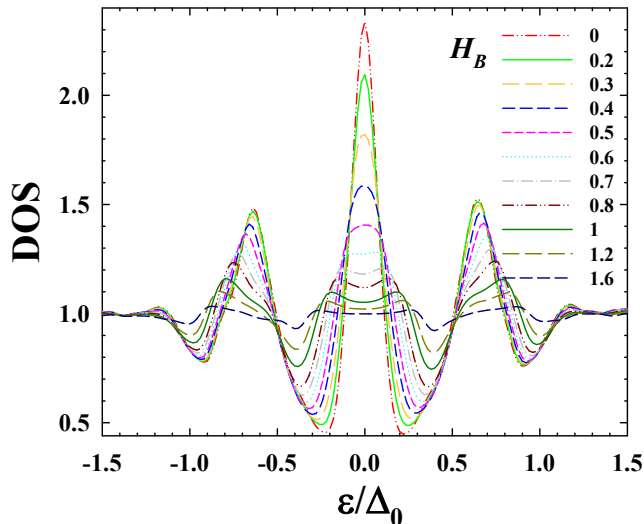


FIG. 9. (Color online) Evolution of the ZEP with scattering strength H_B : The normalized local DOS is shown as a function of the dimensionless energy. Each curve depicts results for a different scattering strength H_B (see text). The system parameters correspond to $D_{F1} = 10$, and $h/\varepsilon_F = 0.1$. The exchange fields in the ferromagnets are mutually orthogonal with $\beta_1 = 90^\circ$, and $\beta_2 = 0^\circ$.

towards the P ($\beta_1 = 0^\circ$) or AP ($\beta_1 = 180^\circ$) alignments, both the triplet amplitude f_1 and the ZEP decline until $\beta_1 = 0^\circ$ or 180° , whereby $f_1 = 0$, and the ZEP has vanished.

Finally, in Fig. 9 we examine the effects of interface scattering on the self-consistent energy spectra. We assume that each interface has the same delta function potential barrier with dimensionless scattering strength H_B . We consider a broad range of H_B , from transparent interfaces with $H_B = 0$, to very high interfacial scattering, with $H_B = 1.6$. By allowing H_B to vary, we effectively control the proximity effects: a small H_B results in stronger proximity coupling between the F and S regions, while a large H_B results in isolation of each segment, and weak proximity effects. This is evident in the DOS, as seen in Fig. 9, which has its largest ZEP when $H_B = 0$. The width and height of the ZEP is strongly influenced by the presence of interface scattering. Increasing H_B results in the ZEP widening while gradually diminishing in height. Eventually, when the scattering strength reaches $H_B \approx 0.7$, the peak begins to split. Further increments in H_B causes the peaks to separate and eventually proximity effects are so weakened that the DOS becomes that of an isolated bulk ferromagnet. The two secondary subgap peaks that lie symmetrically about the ZEP are seen to also decline in a monotonic fashion as H_B becomes larger.

B. Diffusive Regime

In this section, we consider a diffusive SFF junction in the full proximity limit. We employ the Usadel approach described in Sec. II to investigate the local DOS. As remarked

earlier, the quasiclassical method is limited to energies close to the Fermi level. Hence, our discussion here will be limited to relatively weak ferromagnets. As in the ballistic regime, we consider heterostructures where the magnetic layers are made of identical materials so that the ferromagnetic coherence lengths are the same, $\xi_{F1} = \xi_{F2} \equiv \xi_F$, and we consider the low temperature regime where $T = 0.05T_c$. Prior to calculating the DOS, we normalize the Usadel equation by ξ_F , which in the diffusive regime is written, $\xi_F = \sqrt{D/\hbar}$. Using this normalization scheme, the explicit dependency on the exchange field is removed and the Usadel equation now involves terms containing the ratio d_F/ξ_F . This approach can lead to easier pinpointing of regions in parameter space where the ZEP is most prominent, and it also permits a broad range of this ratio to be studied. We assume that the magnetic orientation angle is fixed at $\beta_2 = 0$, or equivalently $\mathbf{h} = (0, 0, h_z)$.

We numerically solve the Usadel equation, Eq. (10), together with the mentioned boundary conditions. To find the total Green's function, we substitute the solution into Eq. (10) and obtain the DOS. To determine the optimal geometry in which the ZEPs are most pronounced, we present in Fig. 10 the ZEP at the topmost edge of the SFF structure, corresponding to the location $x = d_{F1} + d_{F2}$. The two-dimensional color mapping depicts the strength of the DOS at zero energy (the ZEP) as a function of the normalized F thicknesses, d_{F1}/ξ_F and d_{F2}/ξ_F . In the top row panels, the internal field of the F layers have a misalignment angle of $\beta_1 = \pi/2$, while for the bottom row $\beta_1 = \pi/6$. The left, middle, and right columns are for different opacities at the SF interface: $\zeta = 1.0, 2.5$, and 5.0 , respectively. By increasing ζ , the overall strength of the proximity effects is effectively weakened: it is evident that transparent SF contacts yield stronger ZEPs, that persist in thicker F layers. It is also apparent that the orthogonal case $\beta_1 = \pi/2$ has more extensive regions in the parameter space spanned by the F thicknesses with enhanced ZEPs, as compared to the $\beta_1 = \pi/6$ case. An important aspect of the ZEP that all cases investigated in Fig. 10 share, is that it is strongest when $d_{F1} \ll d_{F2}$. This finding is fully consistent with low proximity bilayer SFF hybrids.⁴⁸ Therefore, for the parameters considered here, the ZEPs are strongest for $\zeta = 1, 0.5\xi_F \lesssim d_{F1} \lesssim \xi_F$, and $1.5\xi_F \lesssim d_{F2} \lesssim 3.5\xi_F$. The ratio of the F thickness to the length scale ξ_F is an important dimensionless quantity that appears in the normalized Usadel equations, and consequently thinner d_{F1} and d_{F2} , allow for stronger ferromagnets when studying the DOS in the diffusive limit.

Finally, we study the sensitivity of the ZEPs to both the orientation angle β_1 and interface transparency parameter ζ . We thus show in Fig. 11 the ZEP as a function of β_1 over a wide range of ζ , as shown in the legend. The geometric parameters correspond to $d_{F1} = 0.85\xi_F$ and $d_{F2} = 3.5\xi_F$, which resides within the range of system widths studied in Fig. 10 resulting in the largest ZEPs. In calculating the ZEP, we again consider the DOS at the edge of the sample (see also Fig. 1). It is seen that the interface transparency can significantly alter the behavior of the ZEP as the relative exchange field angle sweeps from the P ($\beta_2 = 0^\circ$) to AP ($\beta_2 = 180^\circ$) orientations. For example, when $\zeta = 1.0$, the maximal ZEP is offset from the

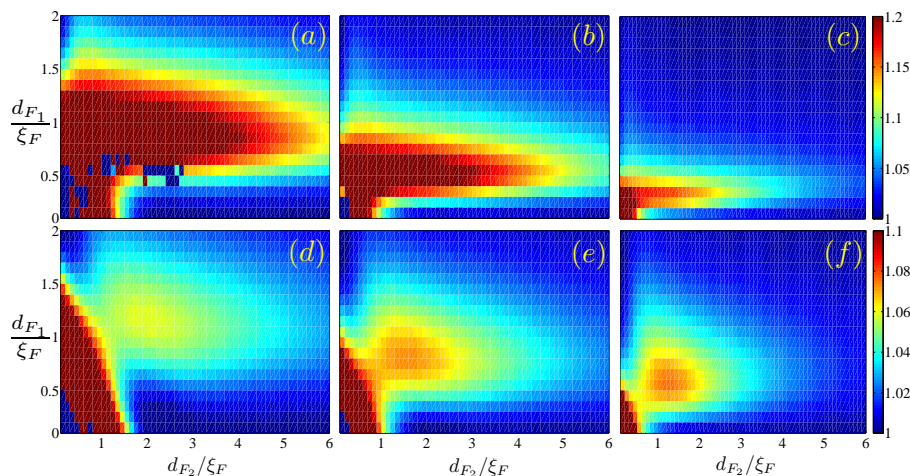


FIG. 10. (Color online) Zero energy peak in the DOS spectrum of diffusive SFF spin valves as a function of the normalized F layer thicknesses d_{F1}/ξ_F and d_{F2}/ξ_F . Each column corresponds to a different SF transparency, with $\zeta = 1, 2.5, 5$ (from left to right). The top row of panels shows the evolution of the ZEP for the misalignment angle $\beta_1 = \pi/2$, while the bottom row of panels are for $\beta_1 = \pi/6$. For both cases, the internal field of the F_2 layer is along the z direction, $\beta_2 = 0$. The ZEPs are computed at $x = d_{F1} + d_{F2}$ (at the top most F /vacuum interface).

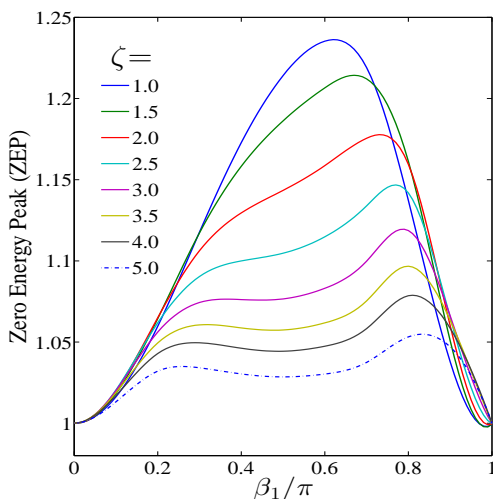


FIG. 11. (Color online) Zero energy peak of the DOS spectrum in diffusive SFF spin valves as a function of exchange field orientation β_1 for several values of ζ , which controls the opacity of the SF interface. We set $\beta_2 = 0$ and rotate the exchange field direction of F_1 from the parallel ($\beta_1 = 0$) to antiparallel ($\beta_1 = \pi$) orientations. We have chosen representative values of $d_{F1} = 0.8\xi_F$ and $d_{F2} = 3.5\xi_F$, in accordance with the system parameters used in Fig. 10.

orthogonal configuration, occurring at $\beta_2 \approx 0.6\pi$. By increasing the barrier strength, this peak shifts towards larger β_2 , until the relative exchange fields are nearly antiparallel. There is also a simultaneous reduction in amplitude, due to the F and S regions becoming decoupled as the proximity effects diminish. Interestingly, as ζ increases, there is a splitting of the main peak: weaker secondary peaks emerge. Eventually however, for sufficiently large ζ , the opacity of the interface causes the low energy DOS to be insensitive to β_1 , and the ZEP flattens out. The ZEPs are also observed to disappear when the relative exchange fields are collinear, corresponding to the situation when the triplet amplitudes vanish in both the diffusive and ballistic regimes (see also Fig. 4).

IV. SUMMARY AND CONCLUSIONS

In summary, we have employed a microscopic self-consistent wavefunction approach to study the low energy proximity induced local DOS in SFF spin valves with non-collinear exchange fields in the clean limit. Our emphasis has been on the results of STM methods that probe the outer F layer. To identify the physical source of the corresponding ZEPs that occurs for such data in these systems, we also calculated the absolute value of the triplet pair correlations, averaged over the outer F layer. We have done so for a broad range of experimentally relevant parameters, including the exchange field strength and orientation, as well as thicknesses of the ferromagnets. Our results demonstrate a direct link between the spin-1 triplet correlations and the appearance of ZEPs in the local DOS spectra, and point to system parameters and configurations which would support larger equal-spin triplet superconducting correlations. These correlations could then be probed indirectly via single-particle signatures that are measurable using local spectroscopy techniques. Our results are consistent with³⁸ findings relating the average strength of triplet correlations to the angular dependence of the transition temperature. Our findings suggest that the ZEPs arising from the spin-1 triplet amplitudes can be effectively isolated in SFF systems with strong ferromagnets, with the outer one being very thin. This asymmetric geometry not only produces greater equal-spin triplet generation, but it can also filter out the rapidly decaying opposite-spin pairs deep within the sample. We also considered the same valve structure in the diffusive regime utilizing a Green function method within the full proximity limit. Our investigations yielded a broad range of F layer thicknesses and relative exchange fields orientations that lead to observable signatures in the low energy DOS, thus also giving useful guidelines for future experiments.

ACKNOWLEDGMENTS

K.H. is supported in part by ONR and by a grant of super-computer resources provided by the DOD HPCMP. We thank N. Birge for many useful discussions about the ZEP problem

and for providing thoughtful feedback on a draft of this work.

M.A. would like to thank A.A. Zyuzin for helpful discussions.

- * phymalidoust@gmail.com
 † klaus.halterman@navy.mil
 ‡ otvalls@umn.edu; Also at Minnesota Supercomputer Institute, University of Minnesota, Minneapolis, Minnesota 55455, USA
- ¹ A. Buzdin, *Rev. Mod. Phys.* **77**, 935 (2005).
 - ² F.S. Bergeret, A.F. Volkov, K.B. Efetov, *Rev. Mod. Phys.* **77**, 1321 (2005).
 - ³ V. L. Berezinskii, *JETP Lett.* **20**, 287 (1975).
 - ⁴ K. Halterman, P.H. Barsic and O.T. Valls, *Phys. Rev Lett.* **99**, 127002 (2007).
 - ⁵ V. P. Mineev and K. V. Samokhin, *Introduction to Unconventional Superconductivity* (Gordon and Breach, Amsterdam) (1999).
 - ⁶ Y. Maeno, H. Hashimoto, K. Yoshida, S. Nishizaki, T. Fujita, J. G. Bednorz, and F. Lichtenberg, *Nature* **372**, 532 (1994).
 - ⁷ V. V. Ryazanov, V. A. Oboznov, A. V. Veretennikov, and A. Yu. Rusanov, *Phys. Rev.* **B65**, 020501 (2001).
 - ⁸ V.V. Ryazanov, V. A. Oboznov, A.Yu. Rusanov, A.V. Veretennikov, A. A. Golubov, and J. Aarts, *Phys. Rev. Lett.* **86**, 2427 (2001).
 - ⁹ K. Halterman, O. T. Valls, *Physica C* **420** 111 (2005).
 - ¹⁰ F.S.Bergeret, A.F. Volkov, K.B.Efetov, *Phys. Rev.* **B65**, 134505 (2002).
 - ¹¹ A. Konstandin, J. Kopu, and M. Eschrig, *Phys. Rev.* **B72**, 140501(R) (2005).
 - ¹² M. Alidoust, G. Rashedi, J. Linder, and A. Sudbø, *Phys. Rev.* **B82**, 014532 (2010).
 - ¹³ R. Fazio and C. Lucheroni, *Europhys. Lett.* **45** 707 (1999).
 - ¹⁴ M. Giroud, H. Courtois, K. Hasselbach, D. Mailly, and B. Pannetier, *Phys. Rev.* **B58**, R11872(1998).
 - ¹⁵ M. Vinet, C. Chapelier, and F. Lefloch, *Phys. Rev.* **B63**, 165420 (2001).
 - ¹⁶ J. Aumentado and V. Chandrasekhar, *Phys. Rev.* **B64**, 054505 (2001).
 - ¹⁷ S. V. Dubonos, A. K. Geim, K. S. Novoselov, and I. V. Grigorieva, *Phys. Rev.* **B65**, 220513 (2002).
 - ¹⁸ A. K. Gupta, L. Cretinon, N. Moussy, B. Pannetier, and H. Courtois, *Phys. Rev.* **B69**, 104514 (2004)
 - ¹⁹ W. Escoffier, C. Chapelier, N. Hadacek, and J.-C. Villegier, *Phys. Rev. Lett.* **93**, 217005 (2004).
 - ²⁰ H. le Sueur, P. Joyez, H. Pothier, C. Urbina, and D. Esteve, *Phys. Rev. Lett.* **100**, 197002 (2008).
 - ²¹ F. Zhou, P. Charlat, B. Spivak, and B. Pannetier, *J. Low Temp. Phys.* **110**, 841 (1998).
 - ²² T. T. Heikkilä, J. Särkkä, and F. K. Wilhelm *Phys. Rev. B* **66**, 184513 (2002)
 - ²³ M. Alidoust, K. Halterman, J. Linder, *Phys. Rev.* **B88**, 075435 (2013).
 - ²⁴ K. M. Boden, W. P. Pratt Jr., and N. O. Birge, *Phys. Rev.* **B84**, 020510(R) (2011).
 - ²⁵ S. Guéron, H. Pothier, N. O. Birge, D. Esteve, and M. H. Devoret, *Phys. Rev. Lett.* **77**, 3025 (1996).
 - ²⁶ H. Pothier, S. Guéron, N. O. Birge, D. Esteve, and M. H. Devoret, *Phys. Rev. Lett.* **79**, 3490 (1997).
 - ²⁷ V. T. Petrashov, I. A. Sosnin, I. Cox, A. Parsons, and C. Troadec, *Phys. Rev. Lett.* **83**, 3281 (1999).
 - ²⁸ T. Kontos, M. Aprili, J. Lesueur, and X. Grison, *Phys. Rev. Lett.* **86**, 304 (2001).
 - ²⁹ I. Sosnin, H. Cho, V. T. Petrashov, and A. F. Volkov, *Phys. Rev. Lett.* **96**, 157002 (2006).
 - ³⁰ C.T. Wu, O.T. Valls, and K. Halterman, *Phys. Rev. Lett.* **108**, 117005 (2012).
 - ³¹ C.T. Wu, O.T. Valls, and K. Halterman, *Phys. Rev.* **B86**, 184517 (2012).
 - ³² M. Alidoust and K. Halterman, *J. Appl. Phys.* **117**, 123906 (2015).
 - ³³ S. Oh, D. Youm, and M. R. Beasley, *Appl. Phys. Lett.* **71**, 2376 (1997).
 - ³⁴ Ya. V. Fominov, *et al.*, *JETP Letters* **91**, 308 (2010).
 - ³⁵ T. Y. Karminskaya, A. A. Golubov, and M. Y. Kupriyanov, *Phys. Rev. B* **84**, 064531 (2011).
 - ³⁶ P.G. de Gennes, *Superconductivity of Metals and Alloys*, (Addison-Wesley, reading, Massachusetts, 1989).
 - ³⁷ C.-T. Wu, O.T. Valls and K. Halterman, *Phys. Rev.* **B86**, 014503 (2012).
 - ³⁸ A.A. Jara, C. Safranski, I.N. Krivorotov, C. Wu, A.N. Malmikakkada, O.T. Valls, and K. Halterman, *Phys. Rev.* **B89**, 184502 (2014).
 - ³⁹ P.V. Leksin, N.N. Garifyanov, I.A. Garifullin, Ya.V. Fominov, J. Schumann, Y. Krupskaya, V. Kataev, O.G. Schmidt, and B. Büchner, *Phys. Rev. Lett.* **109**, 057005 (2012).
 - ⁴⁰ P.V. Leksin, N.N. Garifyanov, I.A. Garifullin, J. Schumann, V. Kataev, O.G. Schmidt, and B. Büchner, *Phys. Rev. Lett.* **106**, 067005 (2011).
 - ⁴¹ P.V. Leksin, N.N. Garifyanov, I.A. Garifullin, J. Schumann, V. Kataev, O.G. Schmidt, and B. Büchner, *Phys. Rev. B* **85**, 024502 (2012).
 - ⁴² P.V. Leksin, N.N. Garifyanov, I.A. Garifullin, J. Schumann, H. Vinzelberg, V. Kataev, R. Klingeler, O.G. Schmidt and B. Büchner, *Appl. Phys. Lett.* **97**, 102505 (2010).
 - ⁴³ K. Usadel, *Phys. Rev. Lett.* **25**, 507 (1970); A.I. Larkin and Y.N. Ovchinnikov, in *Nonequilibrium Superconductivity*, edited by D. Langenberg and A. Larkin (Elsevier, Amsterdam, 1986), P. 493.
 - ⁴⁴ K. Halterman and O.T. Valls, *Phys. Rev. B* **65** 014509 (2002).
 - ⁴⁵ K. Halterman, O.T. Valls and P. H. Barsic, *Phys. Rev.* **B77**, 174511 (2008).
 - ⁴⁶ A. V. Zaitsev, *Zh. Eksp. Teor. Fiz.* **86**, 1742 (1984) (*Sov. Phys. JETP* **59**, 1015 (1984); M. Y. Kupriyanov *et al.*, *Sov. Phys. JETP* **67**, 1163 (1988).
 - ⁴⁷ E. A. Demler, G. B. Arnold, and M. R. Beasley, *Phys. Rev. B* **55**, 15174 (1997).
 - ⁴⁸ M. Alidoust and K. Halterman, *Appl. Phys. Lett.* **105**, 202601 (2014).
 - ⁴⁹ Y.N. Khaydukov, G.A. Ovsyannikov, A.E. Sheyerman, K.Y. Constantinian, L. Mustafa, T. Keller, M.A. Uribe-Laverde, Yu.V. Kisilinskii, A.V. Shadrin, A. Kalabukhov, B. Keimer, D. Winkler, *Phys. Rev. B* **90**, 035130 (2014).
 - ⁵⁰ M. Colci, K. Sun, N. Shah, S. Vishveshwara, D. J. Van Harlingen, *Phys. Rev. B* **85**, 180512(R) (2012); K. Sun, N. Shah, S. Vishveshwara, *Phys. Rev. B* **87**, 054509 (2013).
 - ⁵¹ T. Kontos, M. Aprili, J. Lesueur, and X. Grison, *Phys. Rev. Lett.* **86** (2001).
 - ⁵² S. Kawabata, Y. Asano, Y. Tanaka, and A.A. Golubov, *J. Phys. Soc. of Japan* **82** 124702, (2013).